Theory of nonlinear surface magneto-optics for ferromagnetic nickel: Effects of band structure and matrix elements

W. Hübner*
Institute for Theoretical Physics, Freie Universität Berlin, Arnimallee 14, 1000 Berlin 33, Germany
(Received 1 June 1990)

The nonlinear magneto-optical Kerr effect has been proposed as an ultrafast spectroscopic probe for the magnetic and electronic properties of ferromagnetic surfaces. We extend our previous calculation of the linear (first-order) and nonlinear (second-order) magneto-optical susceptibilities by the inclusion of the complete nickel band structure and the dipole transition matrix elements within the combined interpolation scheme. As *ab initio* band-structure calculations usually cannot describe optical and magneto-optical absorption (especially in nickel), the band-structure parameters are taken from a fit to spin-polarized photoemission data and de Haas–van Alphen measurements of the Fermi surface. The detailed shape of the Brillouin zone is included. Comparison to linear magneto-optical Kerr-effect measurements shows that the inclusion of the full anisotropic band structure and of the dipole matrix elements is necessary to remove parameter ambiguities and leads to strongly improved agreement between theory and experiment. This electronic theory confirms the previous assertion that the nonlinear magneto-optical Kerr effect should be observable and clearly shows that this effect contains detailed information about the electronic and magnetic surface properties (band structure, exchange interaction, spin-orbit coupling). Thus, the theory can help to interpret forthcoming nonlinear magneto-optical measurements. We discuss possible geometries for experimental and technological applications

I. INTRODUCTION

If second-harmonic generation (SHG) occurs at a ferromagnetic surface, the polarization plane of the reflected frequency-doubled photons may be rotated with respect to the incident light polarization. This effect is due to the magnetization of the surface and is called the nonlinear (second-order) magneto-optical Kerr effect. Figure 1 shows a possible experimental setup for this effect which has been proposed as an ultrafast spectroscopic probe for the magnetic and electronic properties of ferromagnetic surfaces[1–3] as it combines the linear (first-order) magneto-optic(al) Kerr effect (MOKE) (which is not surface sensitive) with the surface sensitivity of second-harmonic generation.

In a previous work,[1] we microscopically derived the nonlinear magneto-optical tensor for nickel by an equation-of-motion method and calculated the linear and nonlinear magneto-optical susceptibilities for nickel as a function of the incident photon frequencies. We treated spin-orbit coupling within perturbation theory, used a realistic but simple approximation for the nickel band structure (superposition of spheres in momentum space), and assumed the transition matrix elements to be constant. Lacking nonlinear magneto-optical experiments we checked our assumptions by comparison with linear MOKE spectra and found good agreement between theory and experiment. The theory also showed that the nonlinear magneto-optical Kerr effect should be detectable in surface-SHG experiments.

The aim of this paper is to establish the microscopic theory of the nonlinear magneto-optical Kerr effect from a more-thorough point of view in order to remove any parameter ambiguities. Thus, we extend our previous work in two respects.

(i) We perform a fully three-dimensional anisotropic band-structure calculation to replace the formerly used superposition of three spheres whose radii corresponded to high-symmetry directions.

(ii) We treat the transition matrix elements on the same level as the band structure and use the wave functions resulting from the diagonalization of the Hamiltonian. This problem turns out to be complicated as real- and momentum-space integrations are not separable in this case.

Furthermore, another well-known problem is touched on by our work. There is a remarkable discrepancy between all *ab initio* band-structure calculations and the experimentally determined bands. This difference, which is especially large in the case of nickel (about 1 eV), concerns the positions of the bands in the paramagnetic case, the Fermi-surface shape, and the exchange splitting due to the ferromagnetism of nickel. A lot of work has been

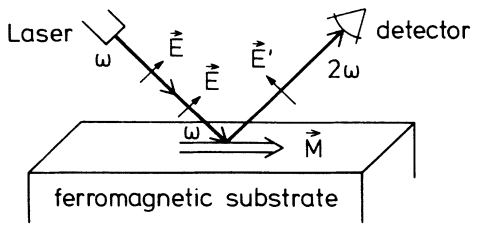

FIG. 1. Possible experimental setup (schematic) for the observation of the nonlinear magneto-optical Kerr effect on a ferromagnetic surface.

done about this problem (e.g., by Liebsch,[4,5] and recently by Nolting,[6] Borgieł,[7] and Gunnarsson and Gies[8]). These discrepancies are conventionally attributed to strong correlations between the nickel d electrons which lead to self-energy or vertex corrections in the susceptibilities. These many-body effects could be treated in the framework of the Hubbard model or by means of the GW extension of *ab initio* calculations and could give rise to shifts, broadenings, and satellites in the band structure. But so far, to our knowledge, no *ab initio* band-structure calculation exists that has solved this problem. Therefore, as we are mainly interested in the calculation of the linear and nonlinear magneto-optical absorption spectra (which are very sensitive to band-structure details and could act as a check for the quality of band-structure calculations), we can neither take advantage of existing *ab initio* band-structure calculations such as that performed by Jepsen *et al.*[9] nor use Slater-Koster parameters which are based on this *ab initio* type of treatment (linear augmented plane-wave technique[10]).

So we take our parameters from a fit to (a) photoemission experiments for the band positions, (b) de Haas–van Alphen data for the Fermi-surface shape, and (c) experimental values of the exchange coupling between the d bands.

As these three types of experiments are independent and contain in a different way some of the important many-body corrections, it is interesting to study to which extent the band structure and the wave functions obtained by the use of those parameters are able to describe magneto-optical absorption spectra (i.e., particle-hole excitations).

Our paper is organized as follows. In Sec. II, we briefly review the basic formulas for the linear and nonlinear magneto-optical susceptibilities in a form we want to use henceforth. In Sec. III, the band-structure calculation is treated, Sec. IV is devoted to the calculation of the matrix elements, in Sec. V we discuss our results for the linear and nonlinear magneto-optical spectra, and in Sec. VI we briefly mention possible experiments and applications of the nonlinear magneto-optical Kerr effect.

II. LINEAR AND NONLINEAR MAGNETO-OPTICAL SUSCEPTIBILITIES

The linear and nonlinear magneto-optical Kerr effects result from the combined action of spin-orbit coupling and exchange interaction. Spin-orbit coupling acts on the electrons like an external magnetic field and thus rotates the polarization plane of linearly polarized light which consists of a superposition of left- and right-handed circularly polarized photons with definite spins -1 or $+1$, respectively. In paramagnets, both electronic spin states are equally occupied and, therefore, the clockwise and counterclockwise rotations cancel. In ferromagnets, however, the exchange interaction splits the band structure, thus leading to an occupation which is different for spin-up and spin-down states. This allows spin-orbit coupling to cause a net rotation of the polarization plane of the light. Therefore, exchange interaction (spin splitting of the band structure) and spin-orbit coupling are important ingredients in our derivation of the linear and nonlinear magneto-optical susceptibilities.

To obtain the *nonlinear* magneto-optical susceptibility $\chi^{(2)}(2\mathbf{q}_\parallel, 2\omega, \mathbf{M})$, we collect the second-order terms in Heisenberg's equation of motion for the density operator. Besides (a) the exchange interaction and (b) spin-orbit coupling, which is about 70 meV in nickel[11,12] and therefore can be treated within perturbation theory, we use the following further ingredients: (c) the band structure of the solid, (d) the dipole transition matrix elements, and (e) the first-order susceptibility $\chi^{(1)}(\mathbf{q},\omega)$, which is the Lindhard function.

Our final result for the nonlinear magneto-optical susceptibility is[3] (up to first order in spin-orbit coupling)

$$
\begin{aligned}
\chi^{(2)}(2\mathbf{q}_\parallel, 2\omega, \mathbf{M}) = \frac{e^3\hbar}{4m^2c^2\mathbf{q}_\parallel^2 A}\sum_\sigma \Bigg(\sum_{\mathbf{k},l,l',l''} \Bigg[\sum_{\mathbf{k}_1} P \Bigg(& \frac{V_{\mathbf{k}_1;\mathbf{k}+2\mathbf{q}_\parallel,l''\sigma}(\mathbf{k}_1 \times (\mathbf{k}+2\mathbf{q}_\parallel)\langle\sigma\rangle)}{E_{\mathbf{k}+2\mathbf{q}_\parallel,l''\sigma} - E_{\mathbf{k}_1}} \\
& \times \langle \mathbf{k}_1 \mid e^{2i\mathbf{q}_\parallel\cdot\mathbf{r}} \mid \mathbf{k}l\sigma\rangle\langle \mathbf{k}l\sigma \mid e^{-i\mathbf{q}_\parallel\cdot\mathbf{r}} \mid \mathbf{k}+\mathbf{q}_\parallel, l'\sigma\rangle \\
& \times \langle \mathbf{k}+\mathbf{q}_\parallel, l'\sigma \mid e^{-i\mathbf{q}_\parallel\cdot\mathbf{r}} \mid \mathbf{k}+2\mathbf{q}_\parallel, l''\sigma\rangle \Bigg) \\
& + Q[V_{\mathbf{k}l\sigma;\mathbf{k}+2\mathbf{q}_\parallel,l''\sigma}(\mathbf{k}\times(\mathbf{k}+2\mathbf{q}_\parallel)\langle\sigma\rangle)\langle \mathbf{k}l\sigma \mid e^{-i\mathbf{q}_\parallel\cdot\mathbf{r}} \mid \mathbf{k}+\mathbf{q}_\parallel, l'\sigma\rangle \\
& \times \langle \mathbf{k}+\mathbf{q}_\parallel, l'\sigma \mid e^{-i\mathbf{q}_\parallel\cdot\mathbf{r}} \mid \mathbf{k}+2\mathbf{q}_\parallel, l''\sigma\rangle] \Bigg] \\
& \times \frac{\left(\dfrac{f(E_{\mathbf{k}+2\mathbf{q}_\parallel,l''\sigma}) - f(E_{\mathbf{k}+\mathbf{q}_\parallel,l'\sigma})}{E_{\mathbf{k}+2\mathbf{q}_\parallel,l''\sigma} - E_{\mathbf{k}+\mathbf{q}_\parallel,l'\sigma} - \hbar\omega + i\hbar\alpha_1} - \dfrac{f(E_{\mathbf{k}+\mathbf{q}_\parallel,l'\sigma}) - f(E_{\mathbf{k}l\sigma})}{E_{\mathbf{k}+\mathbf{q}_\parallel,l'\sigma} - E_{\mathbf{k}l\sigma} - \hbar\omega + i\hbar\alpha_1} \right)}{E_{\mathbf{k}+2\mathbf{q}_\parallel,l''\sigma} - E_{\mathbf{k}l\sigma} - 2\hbar\omega + 2i\hbar\alpha_1} \\
& \times \frac{1}{1 - \dfrac{\pi e^2}{q_\parallel A}\displaystyle\sum_{\mathbf{k},l,l''} |\langle \mathbf{k}l\sigma \mid e^{-2i\mathbf{q}_\parallel\cdot\mathbf{r}} \mid \mathbf{k}+2\mathbf{q}_\parallel, l''\sigma\rangle|^2 \dfrac{f(E_{\mathbf{k}+2\mathbf{q}_\parallel,l''\sigma}) - f(E_{\mathbf{k}l\sigma})}{E_{\mathbf{k}+2\mathbf{q}_\parallel,l''\sigma} - E_{\mathbf{k}l\sigma} - 2\hbar\omega + 2i\hbar\alpha_1}} \Bigg) .
\end{aligned}
\tag{1}
$$

$|\,\mathbf{k}l\sigma\rangle = (1/\sqrt{\Omega})u_{\mathbf{k}l\sigma}e^{i\mathbf{k}\cdot\mathbf{r}}$ are Bloch states of wave vector $\mathbf{k}$ and spin σ in the lth band, $E_{\mathbf{k}l\sigma}$ is their energy, $f(E_{\mathbf{k}l\sigma})$ denotes the Fermi distribution, e is the elementary charge, Ω is the normalization volume, A is the surface area, and the experimental resolution α_1 (which is taken as 0.1 eV throughout) corresponds to the lifetime or imaginary part of the self-energy correction in a many-body theory. $P(\ )$ and $Q(\ )$ denote the permutations of the matrix elements, and the quantity $V_{\mathbf{k}_1;\mathbf{k}+2\mathbf{q}_\parallel,l''\sigma}(\mathbf{k}_1 \times (\mathbf{k}+2\mathbf{q}_\parallel)\langle\sigma\rangle)$ reflects spin-orbit coupling where $V_{\mathbf{k}_1;\mathbf{k}+2\mathbf{q}_\parallel,l''\sigma}$ is the full crystal potential matrix element. The permutations $P(\ )$ refer to the matrix elements with perturbed wave functions whereas the permutations $Q(\ )$ are concerned with the matrix elements of perturbed operators as described in detail in Ref. 3.

It is now possible to simplify the above expression (1) for $\chi^{(2)}(2\mathbf{q}_\parallel, 2\omega, \mathrm{M})$ considerably:

(i) As it was shown in Ref. 3, the nonlinear screening term in the denominator can be neglected if we are interested in laser excitation energies well above 0.5 eV.

(ii) Kittel[13] (see also Argyres[14]) has shown by a simple order-of-magnitude argument that the linear magneto-optical Kerr effect is due to the change of the wave functions by spin-orbit coupling and would be unaffected even if the orbital angular momentum in crystalline nickel would not be completely quenched. In the case of quenching, spin-orbit coupling could not induce any change of the energy levels at all. Thus the transition operators would remain unperturbed. This is of course also true for the *nonlinear* magneto-optical Kerr effect. So we neglect the $Q(\ )$ terms. In the linear case, this argument was confirmed by the numerical analysis and comparison of the $P(\ )$ and $Q(\ )$ terms performed by Wang and Callaway.[11]

(iii) The main contribution to $\chi^{(2)}$ for $\hbar\omega \geq 0.5$ eV comes from interband transitions whereas the Drude (intraband) contribution rapidly dies out (as $1/\omega^2$) and becomes negligible at energies of several hundred millivolts. Thus, we only keep the interband terms within the electric-dipole approximation (in the expansion of the exponentials). Furthermore, SHG experiments clearly demonstrate[15] that higher multipole terms are negligible: The electric quadrupole contribution in linear optics is only of the order of the electric-dipole term in second-harmonic generation.

(iv) The sum over $\mathbf{k}_1$ can be considerably simplified. First, the matrix elements containing $\mathbf{k}_1$ can be replaced by the unperturbed ones. Second, the prefactor

$$\frac{V_{\mathbf{k}_1;\mathbf{k}+2\mathbf{q}_\parallel,l''\sigma}(\mathbf{k}_1 \times (\mathbf{k}+2\mathbf{q}_\parallel)\langle\sigma\rangle)}{E_{\mathbf{k}+2\mathbf{q}_\parallel,l''\sigma} - E_{\mathbf{k}_1}}$$

is replaced by $\lambda_{\mathrm{s.o.}}/\hbar\omega$, where $\lambda_{\mathrm{s.o.}}$ is the spin-orbit constant of the nickel atom, as spin-orbit coupling is a predominantly atomic quantity (which has been confirmed by experiments on nickel clusters). We have shown[3,16] that the sign and the absolute magnitude of the linear and nonlinear magneto-optical susceptibilities calculated within this approach are in excellent agreement with experiment, whereas microscopic calculations of $\lambda_{\mathrm{s.o.}}$ entering for instance surface magnetization anisotropies contradict each other with respect to both sign and magnitude.[17–20] Another justification of our approach can be obtained by replacing the perturbing quantities by their average values

$$\frac{V_{\langle\mathbf{k}_1\rangle;\mathbf{k}+2\mathbf{q}_\parallel,l''\sigma}(\langle\mathbf{k}_1\rangle \times (\mathbf{k}+2\mathbf{q}_\parallel)\langle\sigma\rangle)}{E_{\mathbf{k}+2\mathbf{q}_\parallel,l''\sigma} - \langle E_{\mathbf{k}_1}\rangle}.$$

If we assume for example in the linear case (Fig. 2) that the magnetization is parallel to the z axis (which should be the surface normal of the sample), then $\langle\sigma\rangle = \langle\sigma\rangle_z$. If the incident laser beam is directed parallel to the z axis and the electric photon field is parallel to $\hat{\mathbf{x}}$, the dominant contributions to the perturbation are parallel to the y axis. But they are expected to be small as positive and negative $(\mathbf{k}_1)_y$ occur in the sum (and all angles between $\mathbf{k}_1$ and $\mathbf{k}+2\mathbf{q}_\parallel$ with the weight of the sine function are implicitly present in the cross product).

Moreover, as higher angular momenta usually show more spin-orbit interaction and, on the other hand, the wave functions, belonging to higher angular momenta and being responsible for ferromagnetism, have a more and more atomic character, this perturbation should not be too different from atomic spin-orbit coupling. This simplification can also be justified by numerical calculations (see again Refs. 11 and 12) and by experiments on nickel clusters which show that the magnetism of nickel, in contrast to that of iron, seems to be only slightly affected by the chemical environment of the nickel atoms. Concerning the denominator of this perturbation operator, the energy $\langle E_{\mathbf{k}_1}\rangle$ corresponds to the shift of the eigenvalues due to spin-orbit coupling which is negligible, and $E_{\mathbf{k}+2\mathbf{q}_\parallel,l''\sigma}$ corresponds, on the average, to the excitation energy $\hbar\omega$. Thus we get for the simplified spin-orbit perturbation

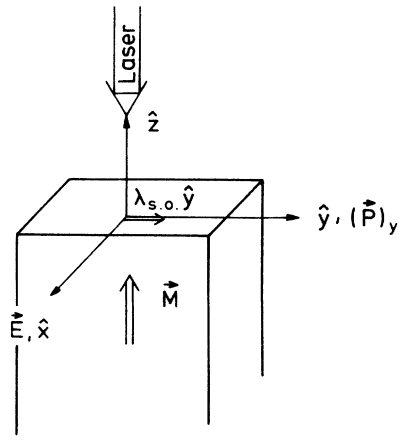

FIG. 2. Illustration of the simplified perturbative inclusion of spin-orbit coupling for a typical linear MOKE experiment in bulk material. The geometry (polar Kerr geometry) corresponds to the measurement of $\omega^2 \mathrm{Im}\chi^{(1)}_{xy}(\omega)$.

$$\frac{\lambda_{\text{s.o.}}}{\hbar\omega - \lambda_{\text{s.o.}}} \approx \frac{\lambda_{\text{s.o.}}}{\hbar\omega} \tag{2}$$

as $\lambda_{\text{s.o.}} \ll \hbar\omega$. This kind of perturbative treatment can be interpreted as replacing, e.g., $\langle \mathbf{k} + 2\mathbf{q}_{\parallel} \mid$ by $(\lambda_{\text{s.o.}}/\hbar\omega)\langle \mathbf{k} + 2\mathbf{q}_{\parallel} \mid$ instead of

$$\sum_{\mathbf{k}_1} \frac{V_{\mathbf{k}_1;\mathbf{k}+2\mathbf{q}_{\parallel},l''\sigma}(\mathbf{k}_1 \times (\mathbf{k} + 2\mathbf{q}_{\parallel})\langle\sigma\rangle)}{E_{\mathbf{k}+2\mathbf{q}_{\parallel},l''\sigma} - E_{\mathbf{k}_1}} \langle \mathbf{k}_1 \mid .$$

Thus, the factor $\lambda_{\text{s.o.}}/\hbar\omega$ measures the relative average strength of the perturbation. By the simplifications (i) through (iv), the complete *nonlinear* magneto-optical susceptibility (which is a tensor of rank 3) reduces to

$$\chi^{(2)}_{xzz}(2\mathbf{q}_{\parallel}, 2\omega, (\mathbf{M})_y)$$

$$= \frac{e^3\hbar}{4m^2c^2\Omega}\frac{\lambda_{\text{s.o.}}}{\hbar\omega}\sum_{\sigma}\sum_{\mathbf{k},l,l',l''}\Bigg(\langle \mathbf{k} + 2\mathbf{q}_{\parallel}, l''\sigma \mid x \mid \mathbf{k}l\sigma\rangle\langle \mathbf{k}l\sigma \mid z \mid \mathbf{k} + \mathbf{q}_{\parallel}, l'\sigma\rangle\langle \mathbf{k} + \mathbf{q}_{\parallel}, l'\sigma \mid z \mid \mathbf{k} + 2\mathbf{q}_{\parallel}, l''\sigma\rangle$$

$$\times \frac{\left(\frac{f(E_{\mathbf{k}+2\mathbf{q}_{\parallel},l''\sigma}) - f(E_{\mathbf{k}+\mathbf{q}_{\parallel},l'\sigma})}{E_{\mathbf{k}+2\mathbf{q}_{\parallel},l''\sigma} - E_{\mathbf{k}+\mathbf{q}_{\parallel},l'\sigma} - \hbar\omega + i\hbar\alpha_1} - \frac{f(E_{\mathbf{k}+\mathbf{q}_{\parallel},l'\sigma}) - f(E_{\mathbf{k}l\sigma})}{E_{\mathbf{k}+\mathbf{q}_{\parallel},l'\sigma} - E_{\mathbf{k}l\sigma} - \hbar\omega + i\hbar\alpha_1}\right)}{E_{\mathbf{k}+2\mathbf{q}_{\parallel},l''\sigma} - E_{\mathbf{k}l\sigma} - 2\hbar\omega + 2i\hbar\alpha_1}\Bigg) . \tag{3}$$

For the *linear* magneto-optical susceptibility, the arguments (ii), (iii), and (iv) give [as (i) is meaningless in that case]

$$\chi^{(1)}_{xy}(\mathbf{q}, \omega, (\mathbf{M})_z) = -\chi^{(1)}_{yx}(\mathbf{q}, \omega, (\mathbf{M})_z)$$

$$= \frac{4\pi e^2}{\Omega}\frac{\lambda_{\text{s.o.}}}{\hbar\omega}\sum_{\mathbf{k},l,l',\sigma}\left[\langle \mathbf{k} + \mathbf{q}, l'\sigma \mid y \mid \mathbf{k}l\sigma\rangle\langle \mathbf{k}l\sigma \mid x \mid \mathbf{k} + \mathbf{q}, l'\sigma\rangle\left(\frac{f(E_{\mathbf{k}+\mathbf{q},l'\sigma}) - f(E_{\mathbf{k}l\sigma})}{E_{\mathbf{k}+\mathbf{q},l'\sigma} - E_{\mathbf{k}l\sigma} - \hbar\omega + i\hbar\alpha_1}\right)\right] . \tag{4}$$

The indices reflect the following geometries. In the linear case, the magnetization $\mathbf{M}$ is parallel to the surface normal which is assumed to be the z direction and the incident beam goes also parallel to $\hat{\mathbf{z}}$, i.e., perpendicular to the surface. Therefore the incident laser field $\mathbf{E}$ is parallel to the $\hat{\mathbf{x}}$ axis and the small Kerr rotation adds a small y component to the polarization. This is usually called the *polar* Kerr geometry for the linear magneto-optical Kerr effect, which probes bulk properties. $\chi^{(1)}_{xy} = -\chi^{(1)}_{yx}$ are the only nonvanishing off-diagonal elements of the rank-two tensor $\chi^{(1)}$. The other off-diagonal elements vanish because of the selection rules $\Delta l = \pm 1$, $\Delta m = 0, \pm 1$ which have to be fulfilled for the two matrix elements. In the case of the nonlinear magneto-optical effect, which probes the topmost surface layer, we choose the magnetization to be in plane ($\parallel \hat{\mathbf{y}}$), the incident beam to be at grazing incidence (i.e., $\mathbf{E} \parallel \hat{\mathbf{z}}$) and the nonlinear Kerr rotation should add a small x component to the polarization. This geometry (p polarization for incident and outgoing photons) takes advantage of the broken symmetry at the surface and gives the highest SHG yield in all experiments.

As spin-orbit coupling is treated within perturbation theory and the exchange interaction is isotropic, the direction of the magnetization is assumed to be fixed by a small externally applied magnetic field which defines the quantization axis as perpendicular to the surface for the linear case and as in plane for the nonlinear case.

The main task is now to determine the band structure and the corresponding wave functions.

III. CALCULATION OF THE NICKEL BAND STRUCTURE

In our previous paper[3] we used a superposition of three spheres, each sphere having the radius of a high-symmetry direction in momentum space. We assumed the band structure to be rotationally symmetric within each sphere and modeled the Brillouin-zone anisotropy by the weight factors attributed to the different spheres. We counted the states correctly by taking care of the factor $k^2\Delta k$ which describes the number of k states in a spherical shell of thickness Δk. The band structure for the high-symmetry directions ΓL, ΓK, and ΓX was taken from the calculation by Weling and Callaway,[21] and the weight factors were chosen such that the experimental linear magneto-optical spectra were reproduced as accurately as possible. This treatment of the band structure corresponds to a Debye approximation for phonons with two exceptions. (1) We used three "Brillouin spheres" instead of only one Debye sphere. (2) Of course, we took some realistic band structure into account (using up to nine bands per spin) instead of assuming just linear dispersion.

Although this approach was successful, we could not exclude some ambiguity or arbitrariness in the choice of the superposition coefficients (called a, b, and c in Ref. 3). Thus, we decided to perform a realistic three-dimensional band-structure calculation to remove possible parameter ambiguities and to compare the spectra to our previous results.

The technique we use is the combined interpolation scheme in the form first proposed by Hodges, Ehrenreich, and Lang[22] and independently in a similar way by Mueller.[23] As this method has also been used by Weling and Callaway,[21] our bands should agree in the high-symmetry directions with theirs. For a detailed review of the method, we refer the reader to the paper by Ehrenreich and Hodges.[24] We mention only some points which we need in our context.

The combined interpolation scheme is a band-structure-calculation method which is especially applicable to transition metals and includes ferromagnetic interactions in a simple way. It forms the basis for the calculation of band structures not only of pure bulk metals but also for alloys, surfaces, clusters, or special geometries. It creates a set of parameters which can be adjusted to experimental data or to *ab initio* band-structure calculations that are not tractable in other than very idealized (usually pure bulk) situations and fail completely in the case of nickel, where they lead to substantial errors of the order of 1 eV (see the Introduction). These errors are not acceptable for the magneto-optical effects as these effects measure the difference of energy differences for both spin directions, which is very sensitive to the details of the band structure.

To set up the Hamiltonian matrix, the philosophy is to use pseudopotentials for the *sp* part and the tight-binding technique in terms of Fletcher-Wohlfahrt[25,26] (instead of the usual Slater-Koster[27]) parameters for the *d* orbitals. The basis set for nickel consists of nine wave functions per spin, namely five linear combinations of atomic orbitals (LCAO's) for the localized $3d$ electrons and four orthogonalized plane waves (OPW's), the latter being in practice just simple plane waves modeling the extended $4s$ and $4p$ states. The OPW's have the form

$$\psi_i(\mathbf{k},\mathbf{r}) = (Nv_a)^{-1/2} e^{i(\mathbf{k}+\mathbf{K}_i)\cdot\mathbf{r}} \quad (i = 1,2,3,4) \tag{5}$$

with $\mathbf{K}_1 = (0,0,0)$, $\mathbf{K}_2 = (0,-16,0)\pi/4a$, $\mathbf{K}_3 = (-8,-8,-8)\pi/4a$, and $\mathbf{K}_4 = (-8,-8,8)\pi/4a$. N is the number of atoms in the solid (which finally will cancel), a is the lattice constant (3.52 Å for nickel), v_a denotes the normalization volume

$$v_a = \frac{a^3}{4Z^3}, \tag{6}$$

$Z = 28$ is the atomic number of nickel, and the factor of 4 corresponds to the four atoms per conventional unit cell of volume a^3 (which contains four times the Brillouin-zone volume in the case of a fcc lattice).

These four plane waves are sufficient for the special $\frac{1}{48}$ of the Brillouin zone which is sufficient for our calculation (for symmetry reasons). The $3d$ LCAO's read

$$\psi_i(\mathbf{k},\mathbf{r}) = N^{-1/2} \sum_l e^{i\mathbf{k}\cdot\mathbf{R}_l} \varphi_i(\mathbf{r}-\mathbf{R}_l) \quad (i = 5,\ldots,9), \tag{7}$$

where the $\phi(\mathbf{r}-\mathbf{R}_l)$ are atomic d orbitals centered at site $\mathbf{R}_l$:

$$\varphi_5(\mathbf{r}) = \left(\frac{15}{4\pi}\right)^{1/2} \frac{xy}{r^2} f(|\,\mathbf{r}\,|),$$

$$\varphi_6(\mathbf{r}) = \left(\frac{15}{4\pi}\right)^{1/2} \frac{yz}{r^2} f(|\,\mathbf{r}\,|),$$

$$\varphi_7(\mathbf{r}) = \left(\frac{15}{4\pi}\right)^{1/2} \frac{zx}{r^2} f(|\,\mathbf{r}\,|),$$

$$\varphi_8(\mathbf{r}) = \left(\frac{15}{16\pi}\right)^{1/2} \frac{x^2-y^2}{r^2} f(|\,\mathbf{r}\,|),$$

$$\varphi_9(\mathbf{r}) = \left(\frac{5}{16\pi}\right)^{1/2} \frac{3z^2-r^2}{r^2} f(|\,\mathbf{r}\,|),$$

where

$$f(|\,\mathbf{r}\,|) = (2\sqrt{2}/3\sqrt{5})(Z/3a_B)^{3/2} \times (Z\,|\,r\,|\,/3a_B)^2 e^{-Z|r|/3a_B}$$

is the normalized radial solution of Schrödinger's equation for the isolated atom and $a_B = 5.29 \times 10^{-11}$ m is Bohr's radius. The normalization condition is $\int_0^\infty [rf(r)]^2 dr = 1$. The nonorthogonality of the atomic orbitals associated with different sites is neglected as it is frequently in the Slater-Koster interpolation scheme. Nevertheless, the d electrons hybridize with the plane-wave *sp* states and therefore an indirect *d-d* interaction comes into play. This special choice of the nine basis functions has two remarkable features.

(1) The set of *sp* orbitals is small enough to avoid a great number of plane waves containing higher reciprocal-lattice vectors.

(2) On the other hand, the set of plane waves is large enough to ensure an appreciable indirect *d-d* interaction, and thus the inclusion of other than nearest-neighbor interactions for the *d*-band portion of the Hamitonian is not necessary. Therefore, concerning the *d-d* Hamiltonian matrix, the combined interpolation scheme in the Fletcher-Wohlfahrt parametrization is equivalent to the orthogonal three-center description of the tight-binding approximation (in Slater-Koster parametrization).

Now we want to discuss the 18×18 Hamiltonian matrix

$$H = \begin{pmatrix} \uparrow\uparrow & 0 \\ 0 & \downarrow\downarrow \end{pmatrix}. \tag{8}$$

As spin-orbit coupling is treated within perturbation theory, different spins are not coupled in the Hamiltonian.

The spin-up and spin-down portions themselves are 9×9 matrices each, e.g.,

$$\uparrow\uparrow = \begin{pmatrix} s\uparrow\, s\uparrow & s\uparrow\, d\uparrow \\ (s\uparrow\, d\uparrow)^\dagger & d\uparrow\, d\uparrow \end{pmatrix}. \tag{9}$$

The three different blocks which are schematically written as $s\uparrow\, s\uparrow$, $s\uparrow\, d\uparrow$, and $d\uparrow\, d\uparrow$ have the forms

$$s\uparrow s\uparrow = \begin{pmatrix} \beta+\alpha\,|\,\mathbf{k}+\mathbf{K}_1\,|^2 & V_{200}\,F_2 & V_{111}\,F_3 & V_{111}\,F_4 \\ V_{200}\,F_2 & \beta+\alpha\,|\,\mathbf{k}+\mathbf{K}_2\,|^2 & V_{111}\,F_2\,F_3 & V_{111}\,F_2\,F_4 \\ V_{111}\,F_3 & V_{111}\,F_2\,F_3 & \beta+\alpha\,|\,\mathbf{k}+\mathbf{K}_3\,|^2 & V_{200}\,F_3\,F_4 \\ V_{111}\,F_4 & V_{111}\,F_2\,F_4 & V_{200}\,F_3\,F_4 & \beta+\alpha\,|\,\mathbf{k}+\mathbf{K}_4\,|^2 \end{pmatrix}. \tag{10}$$

This block corresponds to Harrison's[28] pseudopotential Hamiltonian for aluminum.

The OPW-LCAO block is

$$s\uparrow\ d\uparrow = H_{ij} = B_2 j_2(|\,\mathbf{k}+\mathbf{K}_i\,|\,B_1)\left(\frac{(\mathbf{k}+\mathbf{K}_i)_\mu(\mathbf{k}+\mathbf{K}_i)_\nu}{|\,\mathbf{k}+\mathbf{K}_i\,|^2}\right)F_i(\mathbf{k}),$$

$$(i=1,2,3,4),\ (j,\mu,\nu) = (5,x,y),\ (6,y,z),\ (7,z,x); \tag{11}$$

$$H_{i8} = B_2 j_2(|\,\mathbf{k}+\mathbf{K}_i\,|\,B_1)\left(\frac{(\mathbf{k}+\mathbf{K}_i)_x^2-(\mathbf{k}+\mathbf{K}_i)_y^2}{2\,|\,\mathbf{k}+\mathbf{K}_i\,|^2}\right)F_i(\mathbf{k}); \tag{12}$$

$$H_{i9} = B_2 j_2(|\,\mathbf{k}+\mathbf{K}_i\,|\,B_1)\tfrac{1}{6}\sqrt{3}\left(\frac{3(\mathbf{k}+\mathbf{K}_i)_z^2}{|\,\mathbf{k}+\mathbf{K}_i\,|^2}-1\right)F_i(\mathbf{k}). \tag{13}$$

$j_2(x)$ denotes the spherical Bessel function for angular momentum $l=2$:

$$j_2(x) = \frac{3}{x^3}(\sin x - x\cos x) - \frac{\sin x}{x}. \tag{14}$$

The LCAO-LCAO block $d\uparrow\ d\uparrow$ reads ($\xi = k_x a/2$, $\eta = k_y a/2$, $\zeta = k_z a/2$):

$$H_{55} = E_0 - 4A_1\cos\xi\cos\eta + 4A_2\cos\zeta(\cos\xi+\cos\eta),$$

$$H_{66} = E_0 - 4A_1\cos\eta\cos\zeta + 4A_2\cos\xi(\cos\eta+\cos\zeta),$$

$$H_{77} = E_0 - 4A_1\cos\xi\cos\zeta + 4A_2\cos\eta(\cos\xi+\cos\zeta),$$

$$H_{88} = E_0 + \Delta + 4A_4\cos\xi\cos\eta - 4A_5\cos\zeta(\cos\xi+\cos\eta),$$

$$H_{99} = E_0 + \Delta - \tfrac{4}{3}(A_4+4A_5)\cos\xi\cos\eta + \tfrac{4}{3}(2A_4-A_5)\cos\zeta(\cos\xi+\cos\eta),$$

$$H_{56} = H_{65} = -4A_3\sin\xi\sin\zeta,\ H_{57} = H_{75} = -4A_3\sin\eta\sin\zeta,$$

$$H_{67} = H_{76} = -4A_3\sin\xi\sin\eta,\ H_{58} = H_{85} = 0,$$

$$H_{68} = H_{86} = -4A_6\sin\eta\sin\zeta,\ H_{78} = H_{87} = 4A_6\sin\xi\sin\zeta,$$

$$H_{59} = H_{95} = -\frac{8}{\sqrt{3}}A_6\sin\xi\sin\eta,\ H_{69} = H_{96} = \frac{4}{\sqrt{3}}A_6\sin\eta\sin\zeta,$$

$$H_{79} = H_{97} = \frac{4}{\sqrt{3}}A_6\sin\xi\sin\zeta,\ H_{89} = H_{98} = \frac{4}{\sqrt{3}}(A_4+A_5)\cos\zeta(\cos\eta-\cos\xi).$$

This Hamiltonian contains 14 parameters: The two pseudopotential coefficients, V_{200} and V_{111}, the value β and curvature α of the free-electron bands at the Γ point, the s-d mixing parameters B_2 (which is some hybridization strength) and B_1 [which corresponds to the peak position of the radial function $r^2 f(|\,\mathbf{r}\,|)$], the two d-band-position parameters E_0 and Δ (which reflects crystal field splitting and would be equal to zero within the two-center approximation), and the six Fletcher parameters A_i ($i=1,\ldots,6$) that correspond to the three-center integrals of the tight-binding approximation. The two-center approximation would involve only three Slater-Koster parameters, $(dd\sigma)$, $(dd\pi)$, and $(dd\delta)$. From the technical point of view, the combined interpolation scheme is nearly as ac-

curate as the *nonorthogonal* three-center approximation, but for nickel it is much better because of the parameters which describe photoemission and Fermi-surface data very well (in contrast to the nonorthogonal Slater-Koster parameters given by Papaconstantopoulos[10]).

As future workers for materials different from nickel might be inclined to use Slater-Koster rather than Fletcher parameters, and as we lacked a coherent view of this subject, we give here just the relation between the two parametrizations. (For more details see the original references.)

The Fletcher parameters are defined as follows[26] (V is the crystal potential and U is the atomic potential)

$$A_1 = -\int \varphi_5^*(x-\tfrac{1}{2}a, y-\tfrac{1}{2}a, z)(V-U)\varphi_5(x,y,z)d^3r,$$

$$A_2 = \int \varphi_5^*(x, y-\tfrac{1}{2}a, z-\tfrac{1}{2}a)(V-U)\varphi_5(x,y,z)d^3r,$$

$$A_3 = \int \varphi_5^*(x-\tfrac{1}{2}a, y, z-\tfrac{1}{2}a)(V-U)\varphi_6(x,y,z)d^3r,$$

$$A_4 = \int \varphi_8^*(x-\tfrac{1}{2}a, y-\tfrac{1}{2}a, z)(V-U)\varphi_8(x,y,z)d^3r,$$

$$A_5 = -\int \varphi_8^*(x, y-\tfrac{1}{2}a, z-\tfrac{1}{2}a)(V-U)\varphi_8(x,y,z)d^3r,$$

$$A_6 = \int \varphi_6^*(x, y-\tfrac{1}{2}a, z-\tfrac{1}{2}a)(V-U)\varphi_8(x,y,z)d^3r,$$

and are related to the usual three- and two-center Slater-Koster[24,27] parameters

$$E_0 = -0.95 \text{ eV} = E_{xy,xy}(000) = d_0,$$

$$E_0 + \Delta = -0.890\,640 \text{ eV} = E_{3z^2-r^2,3z^2-r^2}(000) = d_0,$$

$$A_1 = 0.25 \text{ eV} = -E_{xy,xy}(100) = -\tfrac{3}{4}(dd\sigma) - \tfrac{1}{4}(dd\delta),$$

$$A_2 = 0.106\,250 \text{ eV} = E_{xy,xy}(011) = \tfrac{1}{2}(dd\pi) + \tfrac{1}{2}(dd\delta),$$

$$A_3 = 0.121\,385 \text{ eV} = E_{xy,xz}(011) = \tfrac{1}{2}(dd\pi) - \tfrac{1}{2}(dd\delta),$$

$$A_4 = 0.152\,923 \text{ eV} = E_{x^2-y^2,x^2-y^2}(110) = (dd\pi)$$

$$A_5 = 0.015\,131 \text{ eV} = -\tfrac{3}{4}E_{3z^2-r^2,3z^2-r^2}(110) - \tfrac{1}{4}E_{x^2-y^2,x^2-y^2}(110) = -\tfrac{3}{16}(dd\sigma) - \tfrac{1}{4}(dd\pi) - \tfrac{9}{16}(dd\delta),$$

$$A_6 = 0.103\,386 \text{ eV} = \tfrac{1}{2}\sqrt{3}E_{xy,3z^2-r^2}(110) = -\tfrac{3}{8}(dd\sigma) - \tfrac{3}{8}(dd\delta).$$

Weling and Callaway[21] adjusted these 14 parameters of the Hamiltonian at certain symmetry points of the Brillouin zone, where the bands are analytically known, to the photoemission data of Eberhardt and Plummer[29] and to the Fermi-surface measurements of Stark and Tsui.[30,31] Their values for E_0, $E_0+\Delta$, and the A_i ($i = 1,\ldots,6$), which we use, are also given above. The remaining parameter values are $\beta=-8.8$ eV, $\alpha=0.204\,937$ eV$/C^2$, $B_1 = 0.480\,651/C$, $B_2=12.870\,937$ eV, $V_{111}=2.036\,977$ eV, $V_{200}=-0.387\,444$ eV, where $C = \pi/4a$.

The only change of this Hamiltonian matrix induced by ferromagnetism concerns the diagonal elements of the LCAO-LCAO portion. The other portions of the Hamiltonian are identical: $H_{ij} = H_{i+9,j+9}$ ($1 \le i \le 9, 1 \le j \le 9$). Although the experimental exchange splitting is found to be 310 meV,[32] Weling and Callaway found better overall agreement between theory and experiment by using different splittings, namely 400 meV for t_{2g} orbitals and 100 meV for e_g orbitals, which leads to the following band levels: $E_0\downarrow=-0.75$ eV, $E_0\uparrow=-1.15$ eV, $E_0\downarrow+\Delta\downarrow=-0.84$ eV, $E_0\uparrow+\Delta\uparrow=-0.94$ eV. Nevertheless, these values are closer to the experiments than the exchange splitting of 600 to 800 meV of usual *ab initio* band-structure calculations. In addition, this choice of parameters would lead to a reasonable Curie temperature[6] of the order of 630 K and guarantees the reproduction of the magnetic moment of nickel which comes out as 0.5600 Bohr magnetons. To obtain this value in *ab initio* band-structure calculations, it is necessary to compensate for the too low energy of many bands by a larger exchange coupling at the Fermi level.

The omission of the factors $F_i(\mathbf{k})$ ($i = 1,\ldots,4$) occurring in the Hamiltonian [i.e., $F_i(\mathbf{k})=1$] would give rise to shifts and splittings of the bands of the order of the deviation of the combined interpolation scheme bands from those obtained in first-principles computations. These symmetrization factors are calculated in two alternative ways. The first possibility is to use the expressions given by Ehrenreich and Hodges,[24] which lead to a small band-structure discontinuity at the X point. Therefore we alternatively performed a smooth interpolation between the values of the $F_i(\mathbf{k})$ which are known at certain symmetry points [$F_1(\mathbf{k})=1$ everywhere]:

	$F_2(\mathbf{k})$	$F_3(\mathbf{k})$	$F_4(\mathbf{k})$
$\Gamma(0,0,0)$	0	0	0
$X(0,2\pi/a,0)$	1	0	0
$L(\pi/a,\pi/a,\pi/a)$	0	1	0
$K(3\pi/2a,3\pi/2a,0)$	0	1	1
$W(\pi/a,2\pi/a,0)$	1	1	1
$U(\pi/2a,2\pi/a,\pi/2a)$	1	1	0

To do so we divide the $\frac{1}{48}$ of the Brillouin zone, where we have to diagonalize the Hamiltonian, into three disjunct tetrahedra ΓXUW, ΓLUW, and ΓLKW with basis vectors **X**, **U**, **W**, or **L**, **U**, **W**, or **L**, **K**, **W**, respectively. At each **k** point which fulfills the constraint $0 \le k_z \le k_x \le k_y \le 2\pi/a$ we diagonalize three 3×3

matrices to obtain the coordinates of $\mathbf{k}$ in the basis of each of the three tetrahedra. If for any tetrahedron the sum of the coordinates is found in the interval $[0,1]$, the corresponding $\mathbf{k}$ point is contained in this tetrahedron. In this way, we scan the relevant part of the Brillouin zone (which is a truncated octahedron). This procedure automatically reveals the symmetry of each $\mathbf{k}$ point and thus the summation weight for the $\mathbf{k}$ summation in the linear and nonlinear magneto-optical response functions. Usually $\mathbf{k}$ points are found in only one tetrahedron. But if they are found twice or three times then we know that the corresponding $\mathbf{k}$ vector belongs to the interface between two adjacent tetrahedra or the line ΓW (which all tetrahedra participate in), respectively. The coordinates with respect to the tetrahedra are then taken as the coefficients in the linear interpolation of the F functions (which are known at the corners of these tetrahedra). This procedure guarantees a smooth interpolation of $F_i(\mathbf{k})$ and therefore eliminates the discontinuity of the bands at X. Furthermore, it takes care of the detailed anisotropy of the Brillouin zone which has to be taken into account in the $\mathbf{k}$-space summations of the response functions [Eqs.(3) and (4)].

Now all quantities are known to diagonalize the Hamiltonian matrix by using two different numerical standard codes (one of them taken from Papaconstantopoulos[10] and the other being a Householder library routine), both of them leading to the same results. To check our calculated band structure we plotted it in the same high-symmetry directions ΓX, XW, WL, $L\Gamma$, ΓK, and UX as done in Ref. 21 and found perfect agreement of all bands in all directions (within several significant digits at the symmetry points and within plotting accuracy in between) with the results of Weling and Callaway. Our spin-polarized band structure is given in Fig. 3. According to Ref. 21, self-consistency could be achieved by a small shift of the Fermi level by 54.8 meV. The small discontinuity at the X point, which we mentioned before and which also occurs in Ref. 21, can be removed by our alternative interpolation procedure for the $F_i(\mathbf{k})$ (see above).

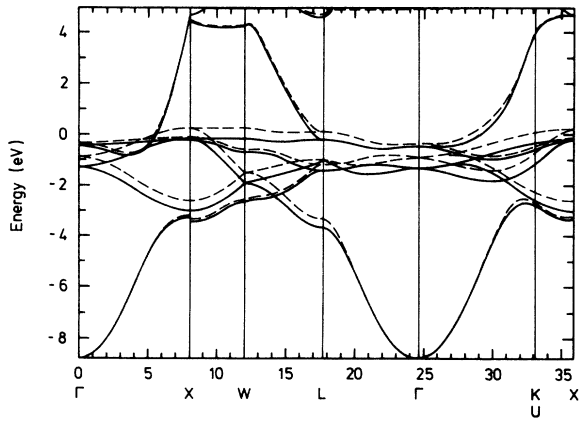

FIG. 3. Spin-polarized nickel band structure, calculated within the combined interpolation scheme (parameters taken from Ref. 21). The solid (dashed) lines are spin-up (spin-down) electrons.

IV. CALCULATION OF THE DIPOLE MATRIX ELEMENTS

In our previous work[1,3,16] we approximated all the matrix elements by the constant value 10^{-11} m. To see at several stages how far our calculated band structure can be taken seriously to describe magneto-optical absorption, we decided to compute also the wave functions and the dipole matrix elements, which enter $\chi^{(1)}$ and $\chi^{(2)}$, from the same Hamiltonian as the band structure. Thus Haydock's[33] recursion method is not applicable to our problem.

The occurring matrix elements have the form $\langle \mathbf{k}l\sigma \mid \hat{O} \mid \mathbf{k}'l'\sigma \rangle$, where the operator $\hat{O}$ stands for the dipole operators x, y, or z and

$$\mathbf{k}' = \mathbf{k} + \mathbf{q}_{(\parallel)} \approx \mathbf{k}$$

or

$$\mathbf{k}' = \mathbf{k} + 2\mathbf{q}_{(\parallel)} \approx \mathbf{k} \text{ as } \mid \mathbf{q}_{(\parallel)} \mid \ll \mid \mathbf{k} \mid .$$

The wave functions $\mid \mathbf{k}'l'\sigma \rangle$ are given as superpositions of the basis functions

$$\Psi_j(\mathbf{k},\mathbf{r}) = \sum_{i=1}^{9} c_{ij}(\mathbf{k}\sigma)\psi_i(\mathbf{k},\mathbf{r}); \quad j = 1,\ldots,9, \tag{15}$$

$$\Rightarrow \langle \mathbf{k}l\sigma \mid \hat{O} \mid \mathbf{k}l'\sigma \rangle = \sum_{i,j} c_{li}(\mathbf{k}\sigma)c_{l'j}(\mathbf{k}\sigma) \times \int \psi_i^*(\mathbf{k},\mathbf{r})\hat{O}\psi_j(\mathbf{k},\mathbf{r})d^3r, \tag{16}$$

where the ψ_i are given by Eqs. (5) and (7), and the coefficient matrices are the diagonalization matrices of the Hamiltonian H

$$C^{\dagger}(\mathbf{k})H(\mathbf{k})C(\mathbf{k}) = E(\mathbf{k}). \tag{17}$$

Thus, the calculation of the band structure $E(\mathbf{k})$ automatically produces the matrix $C(\mathbf{k})$ which contains the complete spin dependence for each point of the Brillouin zone. The remaining task is to determine the spin-independent matrix elements of the basis functions,

$$\int \psi_i^*(\mathbf{k},\mathbf{r})\hat{O}\psi_j(\mathbf{k},\mathbf{r})\, d^3r \ (i = 1,\ldots,9 \text{ and } j = 1,\ldots,9)$$

$$= \frac{1}{N}\sum_{\mathbf{R}_l,\mathbf{R}_l'} e^{-i\mathbf{k}\cdot\mathbf{R}_l} e^{i\mathbf{k}\cdot\mathbf{R}_l'} \int \varphi_i(\mathbf{r}-\mathbf{R}_l)\hat{O}\varphi_j(\mathbf{r}-\mathbf{R}_l')d^3r$$

$$= \frac{1}{N}\sum_{\mathbf{R}_l,\mathbf{R}_l'} \delta_{\mathbf{R}_l,\mathbf{R}_l'}\left(\int \varphi_i(\mathbf{r})\hat{O}\varphi_j(\mathbf{r})\, d^3r + \mathbf{R}_l \int \varphi_i(\mathbf{r})\varphi_j(\mathbf{r})\, d^3r\right)$$

$$= \int \varphi_i(\mathbf{r})\hat{O}\varphi_j(\mathbf{r})d^3r. \tag{18}$$

This holds for an *atomic* basis set. Thus, in the case of an atomic basis (i.e., using hydrogen orbitals φ_i for all ψ_i, including the *sp* functions), the **k** dependence is completely given by the matrices $C(\mathbf{k})$, and the remaining **k**-independent **r** integrals $\int \varphi_i(\mathbf{r})\hat{O}\varphi_j(\mathbf{r})d^3r$ can be computed analytically. We calculated these three-dimensional integrals for all combinations of i and j (i.e., one $4s$, three $4p$, and five $3d$ orbitals) and found the following results:

$$\langle 4p_{m=0} \mid z \mid 4s\rangle = -0.2535 \text{ Å},$$

$$\langle 4p_{m=0} \mid z \mid 3d_{m=0}\rangle = +0.012\,71 \text{ Å},$$

$$\langle 4p_{m=-1} \mid z \mid 3d_{m=-1}\rangle = +0.011\,002\,9 \text{ Å},$$

$$\langle 4p_{m=+1} \mid z \mid 3d_{m=+1}\rangle = +0.011\,002\,9 \text{ Å},$$

$$\left\langle 4p_{m=-1}\left|\begin{pmatrix} x \\ y\end{pmatrix}\right|4s\right\rangle = \begin{pmatrix} 1 \\ i\end{pmatrix}\frac{1}{\sqrt{6}}(0.829\,93)a_B,$$

$$\left\langle 4p_{m=+1}\left|\begin{pmatrix} x \\ y\end{pmatrix}\right|4s\right\rangle = \begin{pmatrix} 1 \\ -i\end{pmatrix}\frac{1}{\sqrt{6}}(0.829\,93)a_B,$$

$$\left\langle 4p_{m=-1}\left|\begin{pmatrix} x \\ y\end{pmatrix}\right|3d_{m=-2}\right\rangle = \begin{pmatrix} 1 \\ -i\end{pmatrix}\frac{1}{\sqrt{5}}(0.046\,509)a_B,$$

$$\left\langle 4p_{m=-1}\left|\begin{pmatrix} x \\ y\end{pmatrix}\right|3d_{m=0}\right\rangle = \begin{pmatrix} -1 \\ -i\end{pmatrix}\frac{1}{\sqrt{30}}(0.046\,509)a_B,$$

$$\left\langle 4p_{m=+1}\left|\begin{pmatrix} x \\ y\end{pmatrix}\right|3d_{m=0}\right\rangle = \begin{pmatrix} -1 \\ i\end{pmatrix}\frac{1}{\sqrt{30}}(0.046\,509)a_B,$$

$$\left\langle 4p_{m=+1}\left|\begin{pmatrix} x \\ y\end{pmatrix}\right|3d_{m=+2}\right\rangle = \begin{pmatrix} 1 \\ i\end{pmatrix}\frac{1}{\sqrt{5}}(0.046\,509)a_B,$$

$$\left\langle 4p_{m=0}\left|\begin{pmatrix} x \\ y\end{pmatrix}\right|3d_{m=-1}\right\rangle = \begin{pmatrix} 1 \\ -i\end{pmatrix}\frac{1}{\sqrt{10}}(0.046\,509)a_B,$$

$$\left\langle 4p_{m=0}\left|\begin{pmatrix} x \\ y\end{pmatrix}\right|3d_{m=+1}\right\rangle = \begin{pmatrix} 1 \\ i\end{pmatrix}\frac{1}{\sqrt{10}}(0.046\,509)a_B.$$

Interchange of the wave functions just leads to the complex conjugate. The other 203 matrix elements vanish. The result corresponds to the atomic selection rules $\Delta l = \pm 1$, $\Delta m = 0, \pm 1$ (see also Sec. II) and gives a crude estimate of the order of magnitude of the matrix elements in the solid.

Unfortunately, the combined interpolation scheme brings an additional complication into play. The *s* and *p* orbitals no longer have atomic character but, on the contrary, are approximated by plane waves. Therefore, the decoupling between **k** and **r** space is no longer possible and Harrison's [34] approximation for the matrix elements does not apply either. Thus, one has to calculate the integrals of the basis functions for each **k** value. Nevertheless, we will show that this task can be considerably simplified because the number of nonvanishing independent complex matrix elements reduces from 162 to 40.

(i) First we show that all the *sp-sp* dipole matrix elements vanish [dipole operator $\hat{O} = \mathbf{r} = (x, y, z)$]:

$$\langle sp \mid \mathbf{r} \mid sp'\rangle = \int \psi_i^*(\mathbf{k},\mathbf{r})\mathbf{r}\,\psi_j(\mathbf{k},\mathbf{r})\, d^3r \ (i = 1,\ldots,4; j = 1,\ldots,4)$$

$$= \frac{1}{Nv_a}\int e^{-i(\mathbf{k}+\mathbf{K}_i)\cdot\mathbf{r}}\,\mathbf{r}\, e^{i(\mathbf{k}+\mathbf{K}_j)\cdot\mathbf{r}}\, d^3r$$

$$= \begin{cases} \int \mathbf{r}\, d^3r = 0 \text{ if } \mathbf{K}_i = \mathbf{K}_j \\ \int \mathbf{r}\,\{\cos[(\mathbf{K}_j - \mathbf{K}_i)\cdot\mathbf{r}] + i\,\sin[(\mathbf{K}_j - \mathbf{K}_i)\cdot\mathbf{r}]\}\, d^3r \text{ otherwise.} \end{cases} \tag{19}$$

The integral over the three-dimensional space vanishes for $\mathbf{K}_i = \mathbf{K}_j$, as the **r** and $-\mathbf{r}$ contributions cancel. The same argument holds for the cosine term in the integral if $\mathbf{K}_i \neq \mathbf{K}_j$. Concerning the remaining sine term (for $\mathbf{K}_i \neq \mathbf{K}_j$), one can show by means of the formula[35]

$$\int_u^\infty x^{\mu-1}\sin x\,dx = \frac{i}{2}[e^{-i\pi\mu/2}\Gamma(\mu,iu) - e^{i\pi\mu/2}\Gamma(\mu,-iu)]\,,\ \mathrm{Re}\,\mu > -1 \tag{20}$$

that the integral over the infinite space vanishes due to the oscillatory behavior of the integrand although the absolute value of the latter increases to infinity. Thus any finite numerical integration would lead to a wrong result.

In addition, the *sp* wave functions do not contribute to magnetism.

(ii) Next, we prove that the *d*-*d* dipole matrix elements do not contribute either:

$$\begin{aligned}\langle d \mid \mathbf{r} \mid d'\rangle &= \frac{1}{N}\sum_{\mathbf{R}_l,\mathbf{R}_l'}\int e^{-i\mathbf{k}\cdot\mathbf{R}_l}\varphi_i(\mathbf{r}-\mathbf{R}_l)\mathbf{r}\,e^{i\mathbf{k}\cdot\mathbf{R}_l'}\varphi_j(\mathbf{r}-\mathbf{R}_l')\,d^3r \\ &= \frac{1}{N}\sum_{\mathbf{R}_l,\mathbf{R}_l'}\delta_{\mathbf{R}_l,\mathbf{R}_l'}\int \varphi_i(\mathbf{r}-\mathbf{R}_l)\mathbf{r}\,\varphi_j(\mathbf{r}-\mathbf{R}_l)\,d^3r \\ &= \int \varphi_i(\mathbf{r})\mathbf{r}\,\varphi_j(\mathbf{r})\,d^3r + \frac{1}{N}\sum_{\mathbf{R}_l}\mathbf{R}_l\int\varphi_i(\mathbf{r})\varphi_j(\mathbf{r})\,d^3r = 0\ (5\le i\le 9,\ 5\le j\le 9).\end{aligned} \tag{21}$$

The second term contributes only for $i = j$, as the atomic orbitals are chosen to be orthonormal. But then the sum over all lattice vectors in infinite space gives zero. The first term vanishes because of the angular momentum selection rule $\Delta l = \pm 1$ for atomic wave functions, which is not fulfilled for two *d* orbitals ($l = 2$ for both of them). The integrand factorizes into radial and angular parts and the replacement $\mathbf{r} \rightarrow -\mathbf{r}$ shows that the integral over the angular part vanishes and the radial part depends only on the absolute value $|\,\mathbf{r}\,|$.

(iii) Now we show that the $\langle d_i \mid \mathbf{r} \mid sp_j\rangle$ matrix elements can be considerably simplified:

$$\begin{aligned}\langle d_i \mid \mathbf{r} \mid sp_j\rangle &= \frac{1}{N\sqrt{v_a}}\sum_{\mathbf{R}_l} e^{-i\mathbf{k}\cdot\mathbf{R}_l}\int\varphi_i(\mathbf{r}-\mathbf{R}_l)\mathbf{r}e^{i(\mathbf{k}+\mathbf{K}_j)\cdot\mathbf{r}}\,d^3r \\ &= \frac{1}{N\sqrt{v_a}}\left(\sum_{\mathbf{R}_l}e^{i\mathbf{K}_j\cdot\mathbf{R}_l}\int\varphi_i(\mathbf{r})\mathbf{r}e^{i(\mathbf{k}+\mathbf{K}_j)\cdot\mathbf{r}}\,d^3r + \sum_{\mathbf{R}_l}e^{i\mathbf{K}_j\cdot\mathbf{R}_l}\mathbf{R}_l\int\varphi_i(\mathbf{r})e^{i(\mathbf{k}+\mathbf{K}_j)\cdot\mathbf{r}}\,d^3r\right)\end{aligned}$$

$$(\le i\le 9,\ 1\le j\le 4). \tag{22}$$

For fcc nickel, the lattice vectors $\mathbf{R}_l$ are given by

$$\mathbf{R}_l = a = n_1\mathbf{a}_1 + n_2\mathbf{a}_2 + n_3\mathbf{a}_3 = \frac{a}{2}\begin{pmatrix} n_2+n_3 \\ n_1+n_3 \\ n_1+n_2\end{pmatrix}, \tag{23}$$

where the fcc basis vectors are

$$\mathbf{a}_1 = \frac{a}{2}\begin{pmatrix}0\\1\\1\end{pmatrix},\ \mathbf{a}_2 = \frac{a}{2}\begin{pmatrix}1\\0\\1\end{pmatrix},\ \mathbf{a}_3 = \frac{a}{2}\begin{pmatrix}1\\1\\0\end{pmatrix},$$

and n_i ($i = 1,2,3$) are positive or negative integers ($n_i = 0,\pm1,\pm2,\ldots$). Thus the factors $e^{i\mathbf{K}_j\cdot\mathbf{R}_l}$ read

$$e^{i\mathbf{K}_1\cdot\mathbf{R}_l} = 1,\ e^{i\mathbf{K}_2\cdot\mathbf{R}_l} = e^{-2\pi i(n_1+n_3)} = 1,$$

$$e^{i\mathbf{K}_3\cdot\mathbf{R}_l} = e^{-2\pi i(n_1+n_2+n_3)} = 1,$$

$$e^{i\mathbf{K}_4\cdot\mathbf{R}_l} = e^{-2\pi i n_3} = 1.$$

Therefore, the second sum in the angular brackets of (24) vanishes due to the factor $\mathbf{R}_l$, while the first sum gives N times the same contribution,

$$\langle d_i \mid \mathbf{r} \mid sp_j\rangle = \frac{1}{N\sqrt{v_a}}\int d^3r\varphi_i(\mathbf{r})\mathbf{r}e^{i(\mathbf{k}+\mathbf{K}_j)\cdot\mathbf{r}}, \tag{24}$$

where N gets compensated by the normalization constant. So it is only necessary to compute 40 complex matrix elements, namely 5×4=20 for the dipole operators x and y or x and z in the linear and nonlinear magneto-optical response functions $\chi^{(1)}_{xy}(\mathbf{q},\omega,(\mathbf{M})_z)$ and $\chi^{(2)}_{xzz}(2\mathbf{q}_\parallel,2\omega,(\mathbf{M})_y)$, respectively. Again, the interchange of *d* and *sp* functions just introduces the complex conjugate of the matrix element. The remaining matrix elements are well-behaved as the atomic *d* orbitals are localized in a very narrow range, each Wigner-Seitz cell gives the same contribution, and the sum is normalized to the number of cells in the solid. Furthermore, intraband transitions, which would dominate for small energies ($\hbar\omega \le 0.5$ eV), are neglected (see Sec. II C). Thus, the singularities mentioned by Aspnes[36] and Moss *et al.*[37] cancel in our dipole matrix elements due to this analytical treatment which takes care of the special symmetry, periodicity, and localization properties of the basis set. But, on the other hand, we can take advantage of the localization of 3*d* electrons as the integrand of the matrix elements is appreciable only very close to the position of its maximum value which is of the order of 10^{-11} m. So we need only a few mesh points near that distance, but of course in all directions.

The detailed shape of the nickel Wigner-Seitz cell which is a rhombic dodecahedron can be taken into ac-

count in the form of the disjunct union of 24 tetrahedra. These tetrahedra were formed by the origin and any possible subset of three of the following 14 Wigner-Seitz cell corners:

$$\frac{a}{2}(\pm 1,0,0),\ \frac{a}{2}(0,\pm 1,0),\ \frac{a}{2}(0,0,\pm 1),\ \frac{a}{4}(1,1,\pm 1),$$

$$\frac{a}{4}(1,-1,\pm 1),\ \frac{a}{4}(-1,1,\pm 1),\ \frac{a}{4}(-1,-1,\pm 1).$$

In a similar way as done before with the Brillouin zone, each space point can be represented in the 24 basis sets of the tetrahedra to decide if it is contained in the Wigner-Seitz cell or not. As we performed this procedure it turned out that its effect is negligible because all contributions to the matrix elements which are of considerable weight are found within the Wigner-Seitz cell due to the localized character of the d wave functions. Thus, we omitted this treatment of the Wigner-Seitz cell anisotropy to save computational time.

V. RESULTS AND DISCUSSION

The objective of this section is to discuss the influence of the detailed inclusion of the fully anisotropic band structure and of the **k**-dependent matrix elements on the calculated linear and nonlinear magneto-optical Kerr spectra, i.e., $\omega^2 \mathrm{Im}\chi^{(1)}_{xy}(\mathbf{q},\omega,(\mathbf{M})_z)$ and $\omega^2 \mathrm{Im}\chi^{(2)}_{xzz}(2\mathbf{q}_{\|},2\omega,(\mathbf{M})_y)$. In addition, we want to check how our previous results[3] that were obtained for constant matrix elements and a simple band-structure treatment (superposition of Brillouin spheres) are improved by this detailed electronic theory. Furthermore, we want to see which features of the spectra remain unchanged and look for plausibility arguments for this behavior.

A. Linear spectrum for constant matrix elements

First we calculate the linear magneto-optical susceptibility $\chi^{(1)}_{xy}$ for constant matrix elements in order to see the effect of the inclusion of the three-dimensional band structure alone. The result for $\omega^2 \mathrm{Im}\chi^{(1)}_{xy}(0,\omega,\mathbf{M})$ is shown in Fig. 4 (up to 6 eV). We neglect the **q** dependence in linear theory as for typical optical experiments $|\ \mathbf{q}\ | \ll |\ \mathbf{k}\ |$. The dipole matrix elements are assumed to have the "atomic" value $\langle |\ \mathbf{r}\ | \rangle = 10^{-11}$ m as in Ref. 3. The **k** sum in momentum space is taken over 6206 **k** points within $\frac{1}{48}$ of the Brillouin zone ($0 \le k_z \le k_x \le k_y \le 2\pi/a$). The tetrahedral decomposition of the truncated octahedron (fcc Brillouin zone) is used as described in Sec. III. To check the convergence behavior of the **k** sum we also used summations over 891 and 148 **k** points. It turns out that the main features of the spectrum are visible even for the 148 **k** points sum but the convergence is not particularly good for this small number of points. This convergence problem has already been mentioned by Moss *et al.*[37] To be as accurate as possible, we diagonalize the Hamiltonian at each **k** point and do not use any interpolation. The value of the energy interval (distance between two abscissa points in Fig. 4) is 0.02 eV.

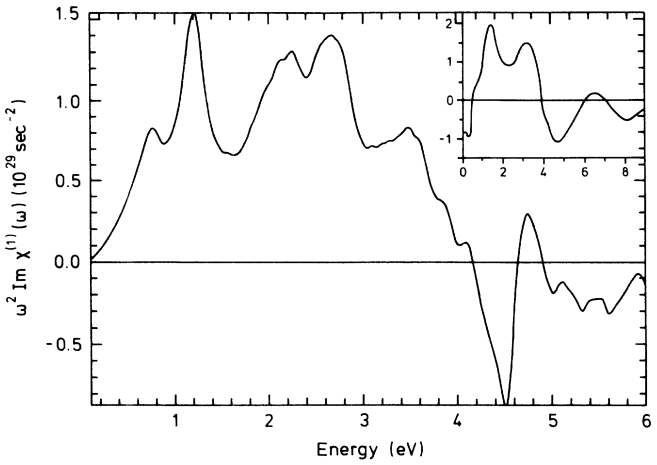

FIG. 4. Linear magneto-optical Kerr susceptibility $\omega^2 \mathrm{Im}\chi^{(1)}_{xy}(\omega)$ for ferromagnetic bulk nickel as a function of frequency ω. The full three-dimensional band structure calculated from the combined interpolation scheme is included but the dipole matrix elements are treated as constants. For comparison, the inset shows a typical experimental result for the same quantity (taken from Ref. 38). The axes are scaled as in the main figure.

The calculated spectrum (in Fig. 4 for 6206 **k** points) clearly shows the same prominent features as the experimental one. There are three peaks centered at 1.2 eV, 2.7 eV (positive sign), and 4.5 eV (negative sign). The corresponding experimental peak positions (depending on the respective experiment) are at 1.15–1.4 eV, 2.7–3.2 eV (positive), and 4.3–4.6 eV (negative), where we have compared to the magneto-optical experiments by Erskine[38] (synchrotron radiation), Yoshino *et al.*,[39] and Krinchik *et al.*[40] (conventional light source). Erskine's spectrum is displayed in the inset of Fig. 4. If we compare the absolute magnitudes of the spectra we find good agreement with experiment. For the height of the first peak, for instance, we obtain 1.55×10^{29} sec^{-2} compared to the experimental value of $(1.2 \text{ to } 2.0)\times10^{29}$ sec^{-2}. In addition, the peak height ratio of the calculated first three peaks [2:1.8:(−1.1)] also agrees well with the experimental value of 2:1.5:(−1) (see Refs. 38 and 40). Furthermore, the peak width ratio of the first two peaks coincides very well with the measurements while our third peak is narrower than the experimental one. Nevertheless, the zero of the experimental spectrum at 3.9 eV is reproduced by our calculation (4.15 eV). Our spectra (which is typical for theory) in general show more details than the experiments which have only finite resolution.

This good overall agreement is in remarkable contrast to *ab initio* calculations where the peak positions deviate from the experiment by more than 1 eV (cf. Sec. I) and the shape of the spectra can hardly be compared with measurements. This clearly demonstrates

that the band-structure parameters derived by Weling and Callaway [21] from photoemission data , de Haas–van Alphen measurements, and spin-polarization experiments also apply very well to the electronic calculation of magneto-optical Kerr spectra. By using this parametrization we effectively include many-body effects (such as self-energy corrections) which are apparently necessary for the interpretation of these magneto-optical excitation spectra. In nickel, the single-particle picture of ordinary density-functional band-structure theory (such as linear augmented plane-wave calculations) is clearly not sufficient for the description of properties other than ground-state properties. Therefore, in the case of nickel (which is probably the most difficult situation for density-functional-based band-structure calculations), our semiempirical band-structure calculation (with the parameters of Ref. 21) gives much better results than *ab initio* calculations[11,41,42] or the fit of the parameters to *ab initio* band structures.[43] Furthermore, as the basic features (magnitude and peak positions) of the magneto-optical spectrum were already visible in our previous work[1,3] based on the superposition of three spherical Brillouin zones, we conclude that our choice of the superposition parameters obviously was not too bad. Therefore, it is clear that the main contributions to the MOKE yield come from the singularities in the joint density of states

$$\rho_{\mathbf{k},l;\mathbf{k}+\mathbf{q},l'}(\hbar\omega) \propto \frac{1}{4\pi^3}\int \frac{dS\,|\langle \mathbf{k}l \mid e^{-i\mathbf{q}\cdot\mathbf{r}} \mid \mathbf{k}+\mathbf{q},l'\rangle|^2}{\nabla_{\mathbf{k}}(E_{\mathbf{k}+\mathbf{q},l'}-E_{\mathbf{k}l})\,|_{E_{\mathbf{k}+\mathbf{q},l'}-E_{\mathbf{k}l}=\hbar\omega}} \qquad (25)$$

which predominantly occur in the high-symmetry directions. Nevertheless, the inclusion of the full three-dimensional nickel band structure leads to considerable improvement concerning the details of the spectrum and removes any ambiguity which may have resulted from the special choice of the superposition coefficients a, b, and c of Refs. 1 and 3.

B. Linear spectrum for k-dependent matrix elements

Next, we include the nonconstant (**k**-dependent) matrix elements calculated as described in Sec. IV to study how the spectrum is modified. The wave functions for the dipole matrix elements are taken from the diagonalization of the same Hamiltonian as the band structure. *A priori*, in an eigenvalue problem, it is not clear that the eigenvectors (wave functions) and matrix elements which reflect the off-diagonal elements of the operator to diagonalize can be taken as seriously as the eigenvalues (energy bands) which reflect the diagonal elements.

For the calculation we again use 6206 **k** points, and the **r**-integration grid for the dipole matrix elements consists of 216 mesh points. We compute the matrix elements between the *basis* functions only once and store them for the rest of the calculation to save computational time. To preserve some kind of selection rules which are lost as the p orbitals are replaced by plane waves in the combined interpolation scheme, we choose the matrix elements (as well as later in the case of the nonlinear spectra) to be invariant under the operation $x\cdot y \rightarrow -x\cdot y$, and keep the exact invariance $z \rightarrow -z$. The abscissa energy interval is now 0.07 eV.

The calculated magneto-optical susceptibility $\omega^2\chi^{(1)}_{xy}(0,\omega,(\mathbf{M})_z)$ which corresponds to the standard polar Kerr geometry (magnetization $\mathbf{M} \parallel \hat{\mathbf{z}}$, incident photon field $\mathbf{E} \parallel \hat{\mathbf{x}}$, light beam directed perpendicular to the surface, outgoing beam obtains small y-polarization component) is displayed in Fig. 5 from 0 to 8 eV. It is obvious from comparison to Fig. 4 that the inclusion of the **k**-dependent matrix elements preserves the general features of the spectrum. The main difference is that the hump, on which the first two peaks are sitting in the case of constant matrix elements, is now missing. The pronounced dip between these peaks is typical for the theoretical spectra containing the **k**-dependent dipole matrix elements (see Refs. 11 and 42). It is hidden in the experiments by the instrumental broadening.

The peak positions remain unchanged. Two further broad peaks centered around 5.5 eV (positive sign) and 7 eV (negative sign) could be attributed perhaps to the features seen by Erskine at 6.5 and 8 eV (inset of Fig. 4). The peak height ratio of 2:1.5:(−1.18) for the first three peaks is even better than before. The absolute value of the first peak maximum is found to be 2.0×10^{29} sec^{-2} and its deviation from its previous value of 1.5×10^{29} sec^{-2} measures the difference between the true average magnitude of the dipole matrix elements and the value of 10^{-11} m assumed in the previous calculations, which was obviously quite realistic.

The width of the peak at 4.5 eV is now considerably

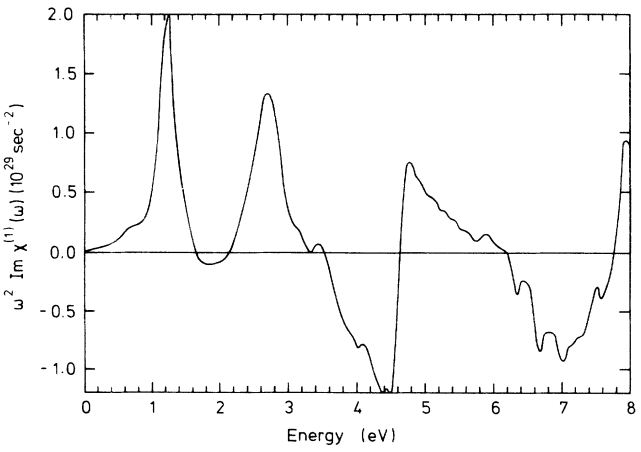

FIG. 5. Linear magneto-optical Kerr susceptibility $\omega^2\mathrm{Im}\chi^{(1)}_{xy}(\omega)$ for ferromagnetic bulk nickel as a function of frequency ω, including the full three-dimensional band structure and the **k**-dependent dipole matrix elements.

enlarged and therefore in better agreement with experiment. The zero between the peaks at 2.7 and 4.5 eV is now found at 3.55 eV, which is 0.35 eV below the experimental value (before it was 0.25 eV above). Concerning most of the features of the spectrum, however, the calculation of the dipole matrix elements on the same footing as the band structure leads to further improved agreement between our theory and the MOKE experiments.

Thus, in general, the inclusion of the *band structure* determines the peak *positions* and the peak *height ratios* whereas the details of the **k**-dependent dipole *matrix elements* are responsible for the *shape* of the peaks and the *absolute magnitude* of the spectrum. This observation is physically plausible as it again confirms the importance of the interband transitions in high-symmetry directions for the occurrence of peaks in the MOKE spectra. To some extent, the effect of the matrix elements averages out due to the admixture of states of different symmetries to the energy levels. So the atomic selection rules are no longer rigorously operating and, roughly speaking, the matrix elements are only *on the average* responsible for the magnitude of the spectra (as they appear in the form of **k**-dependent prefactors in the susceptibilities). The connection to the shape of the peaks (which become narrower by the inclusion of the matrix elements) can be understood in the following way: If one is "off-resonance" the predominance of certain high-symmetry transitions is no longer valid and the "incoherent" behavior of many different matrix elements (also for different spin) leads to a compensation effect which quickly suppresses the pronounced peaks and thus leads to the narrowing effect (in contrast to the "coherent" behavior of constant matrix elements).

The calculated spectra show structures up to 46 eV due to some bands which reach to fairly high energies. But as we did not include *all* bands up to those energies, the calculated spectra can only be taken seriously up to approximately 8 eV. Thus, the abscissas of Figs. 4 and 5 are restricted to this range of energies. Now we want to comment on the negative part which occurs in some of the experimental MOKE spectra at very low frequencies. This feature, which looks rather different in the various MOKE spectra and is not as common a feature as the three prominent peaks, can be due to the following reasons.

(i) Our theory treats spin-orbit coupling within perturbation theory. Thus, there is no real coupling between spin-up and spin-down states. This situation reflects the fact that spin-flip (due to spin-orbit coupling) processes are energetically unfavorable compared to magnon excitation (gapless) which is excluded at zero temperature. This argument is confirmed by the observation that some *ab initio* theories, which find an exchange splitting of approximately 800 meV at the Fermi level (and some shift of the states), show a negative portion of the spectrum up to 1 eV whereas the experimental spectra become positive above 0.5 eV. The possibility of direct spin flips induced by the incident photons due to the $\mathbf{M} \cdot \mathbf{H}$ term of the interaction is negligible, anyway.

(ii) Experimentalists compute the quantity $\omega^2\chi^{(1)}_{xy}(0,\omega,(\mathbf{M})_z)$ from the measured Kerr angles or intensity differences by using formulas which contain optical constants and dielectric functions. Thereby, they neglect the frequency dependence of these quantities which is appreciable in reality.

(iii) Magnons which are excited at room temperature could also rotate the polarization plane of the light at low frequencies.

(iv) The Drude (=intraband) contribution which was neglected in our theory would shift the spectrum by a constant (in vertical direction).

(v) The range below 0.5 eV corresponds to transitions very close to the Fermi level, and our matrix elements may have some uncertainty. Nevertheless, the interesting range for laser experiments and applications is at energies well above 0.5 eV where all these effects do not play any role.

C. Nonlinear spectrum for constant matrix elements

Finally, we calculate the nonlinear magneto-optical susceptibility $\omega^2\chi^{(2)}_{xzz}(2\mathbf{q}_{\|},2\omega,(\mathbf{M})_y)$ for the same semiempirical band structure. If the matrix elements are treated as constants, a prefactor of $|\mathbf{q}_{\|}|a$ has to be introduced in Eq. (3), which ensures that the SHG signal comes exclusively from the topmost surface layer. This factor results from the two-dimensional Fourier transforms and the expansion of the exponentials in the matrix elements of (1). The physical interpretation of this prefactor is the following.

The penetration depth (skin depth) of the incident photons of frequency $\omega = c\mathbf{q}$ is of the order $1/\mathbf{q}_{\|}$. These photons generate field screening processes within this depth that lead to a modified (smoothed out) electronic charge-density profile at the surface. The nonlinear signal results from the interaction of this oscillating surface polarization with the (still impinging) photons of the laser beam. This interaction leads to a radiating surface charge of frequency 2ω and is limited to the screening depth (the depth of broken electronic symmetry at the surface) which is of the order of the topmost layer of surface atoms or less. Thus, the factor $|\mathbf{q}_{\|}|a$ is just the inverse ratio of the photon penetration depth $1/\mathbf{q}_{\|}$ to the second harmonic response depth a (lattice constant). But the details of the electronic charge-density profile at the surface are not very important for the *frequency* dependence of the nonlinear magneto-optical yield, as the latter is mainly due to the "magnetic" d electrons, which are fairly well localized in real space.

As usual the $\mathbf{q}_{\|}$ dependence is neglected in the energy denominators. The truncated bulk approximation is not too bad for nickel, which has nearly ideally flat surfaces (in contrast to the pronounced spin-split surface states of iron, which, on the other hand, follows single-particle behavior of the band structures quite well). Figure 6 shows

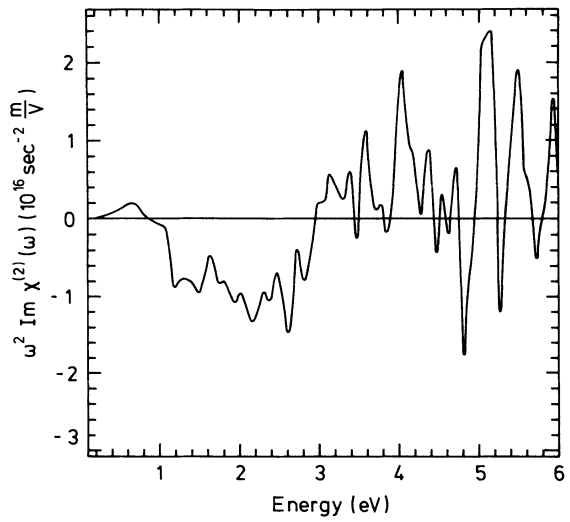

FIG. 6. Nonlinear magneto-optical Kerr susceptibility $\omega^2 \mathrm{Im}\chi^{(2)}_{xzz}(\omega)$ for the surface of ferromagnetic nickel with in-plane magnetization M_y as a function of frequency ω including the full three-dimensional band structure. The dipole matrix elements are treated as constants. The incident and SHG photons are assumed to be p-polarized.

the result for constant matrix elements and abscissa intervals of 0.1 eV. The nonlinear spectrum is of the order of 10^{16} sec^{-2} m/V, which is clearly observable in experiment. The structure of the nonlinear spectrum is much richer than that of the linear magneto-optical susceptibility: Due to the additional intermediate states in the three-photon process, the amount of information is much greater than in the linear Kerr spectrum. The nonlinear magneto-optical Kerr effect measures the difference of spin-up and spin-down state differences between three states ("double difference differences"). So it is very sensitive to the details of the surface electronic structure and to the magnetic surface properties such as magnetization strength and anisotropy, exchange interaction, and spin-orbit coupling.

Although our spectra again (just as in the linear case) show structures up to 46 eV, they should not be taken too seriously above 5–6 eV. In addition, in the nonlinear case the convergence becomes bad for higher energies as we took into account only 891 **k** points within $\frac{1}{48}$ of the Brillouin zone. Nevertheless, at low energies the spectrum which contains the full three-dimensional band structure shows the same basic features as our previous calculation for the superposition of Brillouin spheres: Low-energy peaks occur at 0.6 eV (positive sign), 2.0–2.5 eV (negative), and about 4 eV (positive).

D. Nonlinear spectrum for k-dependent matrix elements

If we include the **k**-dependent matrix elements, we have to omit the prefactor $|\,\mathbf{q}_{\parallel}\,|\,a$ we introduced before, as the surface sensitivity is already contained in the choice of the special tensor element $\chi^{(2)}_{xzz}(2\mathbf{q}_{\parallel}, 2\omega, (\mathbf{M})_y)$ which has been proven to be nonvanishing only on the magnetized surface by group-theoretical tensor classification.[2] The inclusion of the matrix elements in the nonlinear magneto-optical susceptibility (see Fig. 7 for 891 **k** points and abscissa intervals of 0.05 eV) mainly has the same consequences as for the linear Kerr spectra. The overall shape remains unchanged: The peaks again occur at 0.6 eV (positive sign), in a broad range around 2.6 eV (negative), and around 4 eV (positive). Thus, the three-peak structure is a common behavior and is preserved for all nonlinear magneto-optical spectra (for the superposition of Brillouin spheres in Ref. 3, and for the inclusion of the full band structure with constant and **k**-dependent matrix elements). However, one clearly finds that the peaks again become narrower and more structured, which is typical for the effect of the **k**-dependent matrix elements.

The most interesting difference which results from the inclusion of nonconstant matrix elements concerns the absolute magnitude of the susceptibility, which is now of the order of 10^{17} s^{-2} m/V (compared to 10^{16} s^{-2} m/V before). Although this change is not dramatic, it is worthwhile to think about the reasons for it.

Of course, the estimate of 10^{-11} m for the dipole matrix elements is very crude and a small change could induce a big effect on the magnitude of the spectra as the matrix elements enter to the third power. This argumentation also holds for our numerical calculation of the **k**-dependent matrix elements which consist of three triple (i.e., nine single) integrals. Thus, small errors due to the limited ensemble of mesh points would have drastic consequences for the magnitude of the nonlinear Kerr spectra. However, the difference in the magnitude of the non-

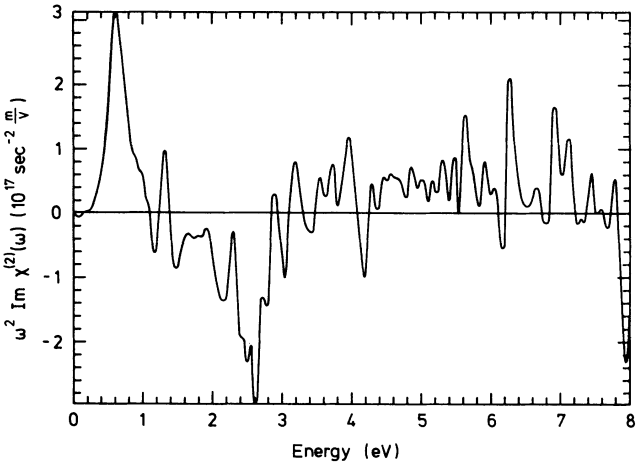

FIG. 7. Nonlinear magneto-optical Kerr susceptibility $\omega^2 \mathrm{Im}\chi^{(2)}_{xzz}(\omega)$ for the surface of ferromagnetic nickel with in-plane magnetization M_y as a function of frequency ω including the full three-dimensional band structure and the **k**-dependent dipole matrix elements. The incident and SHG photons are assumed to be p-polarized.

linear spectra for constant and **k**-dependent matrix elements (which does not occur in the linear case) is probably more tightly connected to the treatment of the surface which, in both cases but in a different way, demonstrates the *surface sensitivity* of the nonlinear magneto-optical Kerr effect.

In the case of *constant* matrix elements, the effect of the surface is reflected by the factor $|\mathbf{q}_{\parallel}|\, a$ whereas we use a modified truncated bulk approximation for **k**-*dependent* matrix elements: This means that the nonlinear Kerr yield, which would exactly vanish in bulk (because of the $z \rightarrow -z$ invariance of the product of the three matrix elements), is entirely due to the cut of the topmost Wigner-Seitz cell. This cut is performed in the middle of the cell (which maximizes the nonlinear yield) and reflects the broken electronic symmetry on the surface which is responsible for SHG. A slight shift (of the order of 0.1 Å) of the crystal cutting line (which in reality occurs by cleaving or by the preparation of a single surface) would reduce the yield (by one order of magnitude) because of compensation effects in different parts of the unit cell.

On the other hand, the wave vector $\mathbf{q}_{\parallel}$ in the factor $|\mathbf{q}_{\parallel}|\, a$ which appears for *constant* matrix elements and has been interpreted above, could be replaced by the plasma wave vector $\mathbf{q}_{\parallel,\mathrm{plasma}}$ which is larger and connects the skin depth to the onset of transparency in (free-electron) metals. This replacement would remove not only the difference in the order of magnitude but also the suppression of the low-energy peaks for constant matrix elements.

In general, however, the magnitude of our calculated nonlinear Kerr spectra is in good agreement with recent SHG experiments and SHG calculations and supports our statement that the nonlinear magneto-optical Kerr effect should be observable in experiment: (a) The ratio of nonlinear magneto-optical susceptibility to ordinary SHG yield was estimated independently by us[1] and by Pan *et al.*[2] as $0.07i$ where i is the imaginary unit. (b) Concerning the absolute value of the nonlinear Kerr susceptibility, our estimate turned out to be in excellent agreement[16] with recent SHG experiments on Al(111) in UHV by Murphy *et al.*[44] and on Ag(111) in electrolytic solution by Guyot-Sionnest[45] which were the first reliable measurements of absolute SHG yields. These yields were confirmed by Liebsch[45] in detailed jellium SHG calculations. (c) In addition, we note that the nonlinear magneto-optical Kerr effect should be observable with already existing experimental equipment in the presence of an external magnetic field even in vacuum without any enhancement by a condensed-matter surface.[46] This altogether supports our statement that the nonlinear magneto-optical Kerr effect should be detectable in surface-SHG experiments (with the yield and frequency dependence given by our calculation) and thus could become a promising tool for the optical analysis of magnetic surface phenomena.

In conclusion, to establish a more-detailed theory of nonlinear surface magneto-optics and to check the influence of the fully anisotropic band structure and of the **k**-dependent dipole transition matrix elements, we calculated in an electronic theory the linear and nonlinear magneto-optical spectra (as a function of frequency) for ferromagnetic nickel. We semiempirically computed the three-dimensional band structure and treated the matrix elements on the same footing. It turned out that the inclusion of the band structure leads to considerably improved agreement between theory and linear MOKE experiments. This agreement clearly shows that the band-structure parameters, derived from (spin-polarized) photoemission data and de Haas–van Alphen measurements, also describe magneto-optical absorption very well. Although some further improvement concerning the peak height ratios and the peak widths is obtained by the inclusion of the matrix elements, the most prominent features of the spectra are already revealed if the matrix elements are taken as constants. However, the inclusion of the matrix elements is necessary to choose special geometries for the experiments. The detailed electronic theory confirms our earlier statements that the nonlinear magneto-optical Kerr effect is surface specific (especially for p-polarized photons) and should be observable in experiment. In general, most of the peaks in the spectra become narrower for **k**-dependent matrix elements. We find that the peak positions and peak height ratios are determined by the band structure (mainly interband transitions in high-symmetry directions) whereas the absolute values and the peak widths are affected by the inclusion of the **k**-dependent matrix elements. The nonlinear magneto-optical Kerr effect is very sensitive to the band-structure details and thus provides a lot of information about the magnetic (exchange interaction, spin-orbit coupling) and electronic properties of ferromagnetic surfaces.

VI. POSSIBLE EXPERIMENTS AND APPLICATIONS

Nonlinear magneto-optical *experiments* can be done in two different ways: Either one measures the frequency dependence of the nonlinear *Kerr rotation* ($\approx 0.1°$ in nickel) directly and extracts the nonlinear magneto-optical susceptibility from it, or one determines *SHG intensity differences* with and without magnetization (e.g., by heating up the sample or by rotating either the sample or the small applied magnetic field). Therefore two extreme experimental geometries (and any setup in between) are conceivable.

(a) In order to keep the SHG signal for the detection of the Kerr angle as large as possible, it is favorable to take advantage of the enhancement by the nonlinearity perpendicular to the surface by using p-polarized incident and p-polarized frequency-doubled outgoing photons. This geometry always gives the highest SHG yield (see, e.g., Ref. 47).

(b) On the other hand, if one is interested in comparing intensities, it is necessary to have a large signal-to-noise

ratio. In that case, it is favorable to use s-polarized incident and s-polarized frequency-doubled outgoing photons. In this geometry, (100) fcc surfaces give (within the electric dipole approximation) no SHG signal at all[2] if there is no magnetization present. Thus, the apparatus could operate with a high signal-to-noise ratio because of the low background (bulk) signal.

Of course, one can also optimize the experimental setup between the two extreme cases (a) and (b) depending on the material, temperature range, etc., under consideration.

As second-harmonic generation has become a useful optical tool for the investigation of the structural and electronic properties of pure and adsorbate-covered surfaces and interfaces,[48–51] the nonlinear Kerr effect could open a field of important and interesting experiments in *basic research* about the magnetic behavior of pure metals, intermetallic alloys, low-dimensional electronic systems, elementary magnetic excitations, Curie temperatures of ultrathin epitaxial magnetic films, or critical thermodynamics.

The very-high-frequency sensitivity can be used to study the magnetic properties of perturbed systems such as adsorbates or layered structures and to follow, in combination with the high time resolution of lasers, the magnetic properties dynamically during selective bond-breaking processes.

As nonlinear optics applies at any interface accessible by light and is nondestructive, it is possible to study, in the presence of an externally applied magnetic field, completely different interesting chemical or biological systems (without exchange interaction and the effect of spin-orbit coupling) such as rigid rod polymers (phase transition from chains to networks), liquid-crystal monolayers,[52] or biological membranes.

Possible technological *applications* (e.g., magneto-optical read-write memories) should combine thermomagnetic laser writing with magneto-optical perpendicular recording. In that case it is necessary to store as many magnetic bits as possible per unit area or maybe per unit volume and to read out this information very fast. So one only needs to know whether there is a bit at a certain position or not. As the domain size (= bit size) is of the order of 100 nm in diameter, it is necessary to use photon energies of the order of several eV. The enormous frequency dependence of the nonlinear magneto-optical Kerr effect together with the high laser frequency selectivity (narrow frequency range) could possibly be used to read out information from different depths in layered magneto-optical memories as these different layers would behave slightly differently by geometry or by preparation (compositional modulation). Thus, a first step towards three-dimensional magneto-optical recording could become possible.

ACKNOWLEDGMENTS

The author gratefully acknowledges stimulating discussions with Professor K.-H. Bennemann. This work has been supported by Sonderforschungsbereich 6 of the Deutsche Forschungsgemeinschaft (Bonn, Germany).

*Present address: Department of Physics, University of California, Berkeley, CA 94720.

[1] W. Hübner and K.-H. Bennemann, Europhys. Conf. Abs. **13A**, A42 (1989).
[2] R.-P. Pan, H.D. Wei, and Y.R. Shen, Phys. Rev. B **39**, 1229 (1989).
[3] W. Hübner and K.-H. Bennemann, Phys. Rev. B **40**, 5973 (1989).
[4] A. Liebsch, Phys. Rev. Lett. **43**, 1431 (1979).
[5] A. Liebsch, Phys. Rev. B **23**, 5203 (1981).
[6] W. Nolting, W. Borgiel, V. Dose, and Th. Fauster, Phys. Rev. B **40**, 5015 (1989).
[7] W. Borgiel and W. Nolting, Z. Phys. B **78**, 241 (1990).
[8] O. Gunnarsson, P. Gies, W. Hanke, and O.K. Andersen, Phys. Rev. B **40**, 12 140 (1989); P. Gies, private communication.
[9] O. Jepsen, J. Madsen, and O.K. Andersen, Phys. Rev. B **26**, 2790 (1982).
[10] D.A. Papaconstantopoulos, *Handbook of the Bandstructure of Elemental Solids* (Plenum, New York, 1986).
[11] C.S. Wang and J.Callaway, Phys. Rev. B **9**, 4897 (1974).
[12] E. Wimmer, A.J. Freeman, and H. Krakauer, Phys. Rev. B **30**, 3113 (1984).
[13] C. Kittel, Phys. Rev. **83**, 208(A) (1951).
[14] P.N. Argyres, Phys. Rev. **97**, 334 (1955).
[15] P. Tepper and J. Reif, private communication.
[16] W. Hübner and K.-H. Bennemann, Vacuum **41**, 514 (1990).
[17] P.J. Jensen and K.-H. Bennemann, Phys. Rev. B **42**, 849 (1990).
[18] A.J. Bennett and B.R. Cooper, Phys. Rev. B **3**, 1642 (1971).
[19] H. Takayama, H.-P. Bohnen, and P. Fulde, Phys. Rev. B **14**, 2287 (1976).
[20] J.P. Gay and R. Richter, Phys. Rev. Lett. **56**, 2728 (1986); J. Appl. Phys. **61**, 3362 (1987).
[21] F. Weling and J. Callaway, Phys. Rev. B **26**, 710 (1982).
[22] L. Hodges, H. Ehrenreich, and N.D. Lang, Phys. Rev. **152**, 505 (1966).
[23] F.M. Mueller, Phys. Rev. **153**, 659 (1967).
[24] H. Ehrenreich and L. Hodges, Methods Comput. Phys. **8**, 149 (1968).
[25] G.C. Fletcher and E.P. Wohlfahrt, Philos. Mag. **42**, 106 (1951).
[26] G.C. Fletcher, Proc. Phys. Soc. (London) **A65**, 192 (1952).
[27] J.C. Slater and G.F. Koster, Phys. Rev. **94**, 1498 (1954).
[28] W.A. Harrison, Phys. Rev. **118**, 1182 (1960).
[29] W. Eberhardt and E.W. Plummer, Phys. Rev. B **21**, 3245 (1980).
[30] D.C. Tsui, Phys. Rev. **164**, 669 (1967).
[31] R.W. Stark and D. C. Tsui, J. Appl. Phys. **39**, 1056 (1968).

[32]D.E. Eastman, F.J. Himpsel, and J.A. Knapp, Phys. Rev. Lett. **40**, 1514 (1978).
[33]R. Haydock, in *Solid State Physics*, edited by H. Ehrenreich, F. Seitz, and D. Turnbull (Academic, New York, 1980), Vol. 35, p. 215.
[34]W.A. Harrison, *Electronic Structure and the Properties of Solids* (Freeman, San Francisco, 1980), p. 118ff.
[35]I.S. Gradshteyn and I.M. Ryzhik, *Table of Integrals, Series, and Products* (Academic, New York, 1965), p.420.
[36]D.E. Aspnes, Phys. Rev. B **6**, 4648 (1972).
[37]D.J. Moss, E. Ghahramani, J.E. Sipe, and H.M. van Driel, Phys. Rev. B **41**, 1542 (1990).
[38]J.L. Erskine, Physica B+C **89B**, 83 (1977).
[39]T. Yoshino and S. Tanaka, Opt. Commun. **1**, 149 (1969).
[40]G.S. Krinchik and V.A. Artemjev, J. Appl. Phys. **39**, 1276 (1969).
[41]N.V. Smith, R. Lässer, and S. Chiang, Phys. Rev. B **25**, 793 (1982).
[42]H. Ebert (unpublished).
[43]W. Hübner (unpublished).
[44]R. Murphy, M. Yeganeh, K.H. Song, and E.W. Plummer, Phys. Rev. Lett. **63**, 236 (1989).
[45]P. Guyot-Sionnest, A. Tadjeddine, and A. Liebsch, Phys. Rev. Lett. **64**, 1678 (1990).
[46]Y.J. Ding and A.E. Kaplan, Phys. Rev. Lett. **63**, 2725 (1989).
[47]G. Marowski, R. Steinhoff, L.F. Chi, J. Hutter, and G. Wagniére, Phys. Rev. B **38**, 6274 (1988).
[48]Y.R. Shen, Ann. Rev. Mater. Sci. **16**, 69 (1986).
[49]G.L. Richmond, J.M. Robinson, and V.L. Shannon, Prog. Surf. Sci. **28**, 1 (1988).
[50]Li Le, Liu Yanghua, Yu Gongda, Wang Wencheng, and Zhang Zhiming, Phys. Rev. B **40**, 10 100 (1989).
[51]T.F. Heinz, F.J. Himpsel, E. Palange, and E. Burstein, Phys. Rev. Lett. **63**, 644 (1989).
[52]W. Chen, M.B. Feller, and Y.R. Shen, Phys. Rev. Lett. **63**, 2665 (1989).